

Supplementary Information

Highly Regio- and Enantioselective Thermal [2+2] Cycloaddition of Coumarin in a Crystalline Inclusion Complex under High Vacuum†

Yongqiang Wen,^a Yanlin Song,^{*a} Dongbo Zhao,^b Kuiling Ding,^{*b} Jiang Bian,^c Xue Zhang,^b Jingxia Wang,^a Yang Liu,^a Lei Jiang,^a and Daoben Zhu^a

Experimental Section:

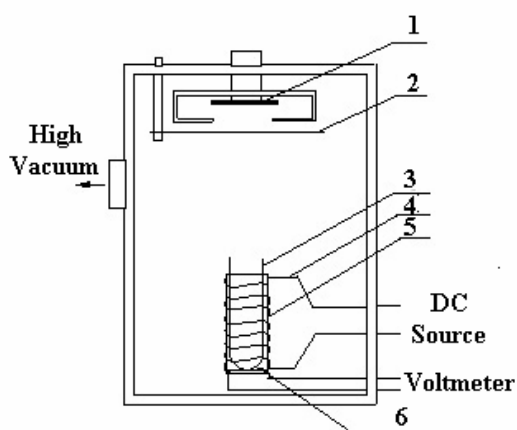


Figure S1 Sketch map of the used experiment apparatus. It is a vapour deposition equipment under high vacuum, without laser-, electron-, or ion-guns. The temperature of the crucible was detected by a thermocouple. **1** - substrate, **2** - baffle, **3** - quartz crucible, **4** - tungsten filament, **5** - porcelain crucible, **6** - thermocouple.

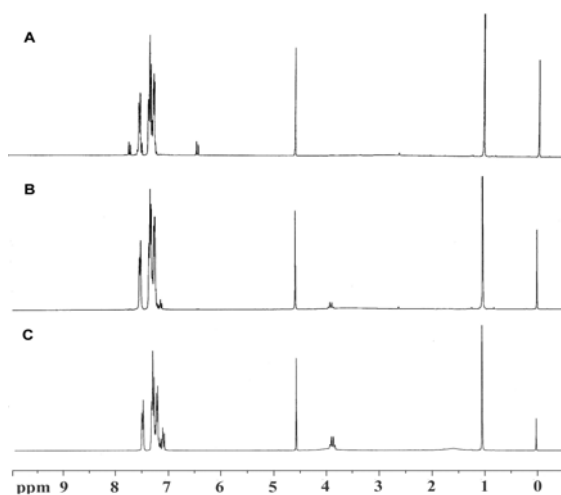


Figure S2 ¹H NMR spectra of inclusion complex **1a** before (A) and after (B) thermal dimerization, as well as the standard sample **2a** obtained by solid-state photochemical dimerization (C). They were recorded on a Bruker DMX-300 instrument. The signals of pyrone moiety protons appeared at 6.42 - 6.45 and 7.70 - 7.73 ppm vanished when inclusion complex **1a** was heated at high vacuum, and simultaneously a set of new peaks of multiplets at 3.87 - 3.96 ppm appeared.

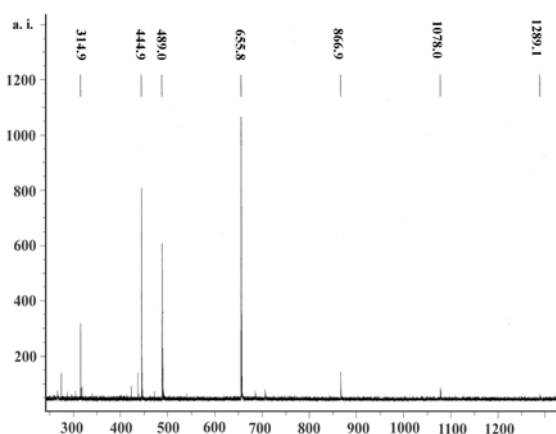


Figure S3 Matrix assisted laser desorption ionization-time of flight (MALDI-TOF) mass spectra of the thermal products. It was determined with BIFLEXIII MALDI-TOF-MS spectrometer. Experimental conditions: positive reflective mode, CCA + Na as matrix. The peaks at 314.9 and 489.0 corresponded to $(M_{\text{coumarin dimer}} + \text{Na})^+$ and $((-)\text{-Taddol} + \text{Na})^+$, respectively.

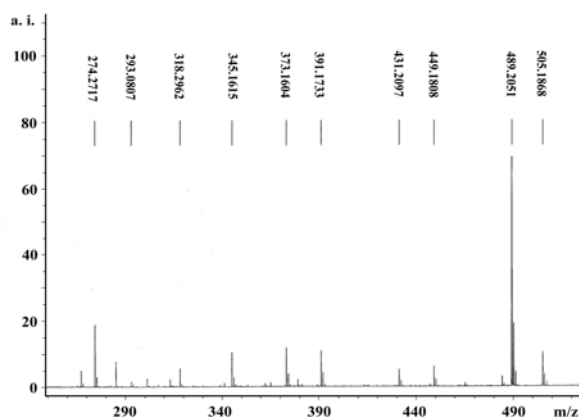


Figure S4 Electrospray ionization (ESI) mass spectra of the thermal products. It was determined with APEXII FT-ICR ESI-MS spectrometers. Experimental condition: positive mode, H_2O -MeOH as solvents. The peaks at 293.0807 and 489.2051 corresponded to $(M_{\text{coumarin dimer}} + \text{H})^+$ and $((-)\text{-Taddol} + \text{Na})^+$, respectively.

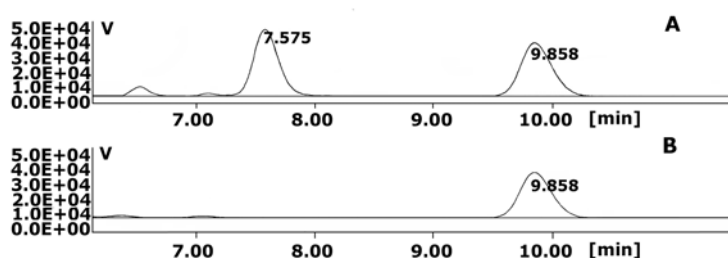
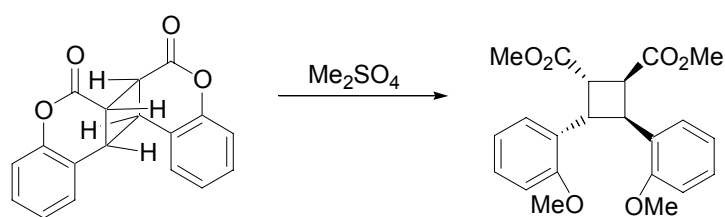


Figure S5 Chiral HPLC of tetramethyl derivative of *anti* head-to-head coumarin dimer. (A) racemic mixture; (B) thermal dimerization derivative. The enantiomeric excess of coumarin was determined by conversion to its tetramethyl derivative by treatment with Me_2SO_4 (as following Supplementary Scheme1) under basic condition with HPLC on a Chiralpak AD column with hexane-isopropanol (85:15) as eluent, flow rate = 0.8 mL/min.



Scheme S1

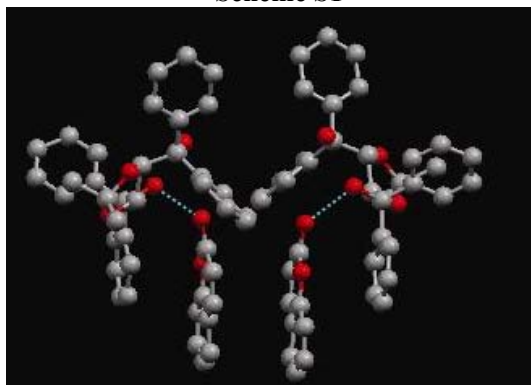


Figure S6 Schematic illustration of two Coumarin molecules relative position in crystalline inclusion complex. The image was generated using MERCURY. The crystal structure of **1a** was previously reported by Tanaka et al.^[1] The crystallographic data can be obtained from Cambridge Structural Database (CSD) (No. CCDC 118773). Copies of the data can be obtained free of charge on application to CCDC, 12 Union Road, Cambridge CB2 1EZ, UK (fax: (+44)1223-336-033; e-mail: deposit@ccdc.cam.ac.uk). Crystal structure of complex **1a**: C₄₀H₃₆O₆, M_r = 612.72, space group monoclinic C₂, a = 35.59(4), b = 9.489(4), c = 10.03(1) Å, β = 102.70(4)°, V = 3305(4) Å³, Z = 4, ρ = 1.23 g cm⁻³, μ = 0.82 cm⁻¹, T = 293K, R = 0.105, R_w = 0.088.

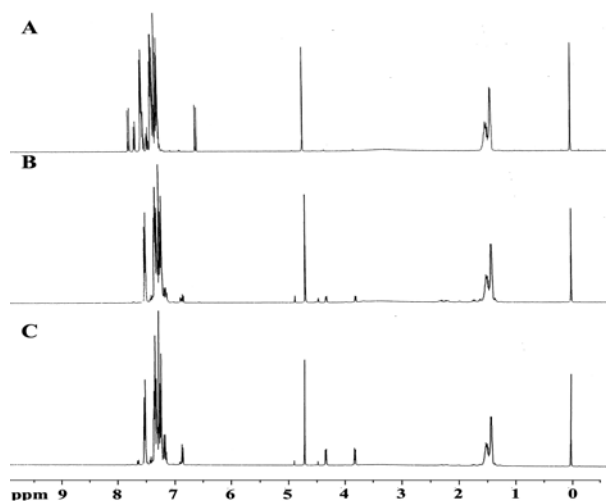


Figure S7 ¹H NMR spectra of inclusion complex **1b** before (A) and after (B) thermal dimerization, as well as the standard sample **2b** obtained by solid-state photochemical dimerization (C). The signals of pyrone moiety protons appeared at 6.54 - 6.57 and 7.71 - 7.73 ppm vanished when inclusion complex **1b** was heated at high vacuum, and simultaneously two sets of new peaks centred at 3.78 - 3.80 and 4.30-4.32 ppm appeared.

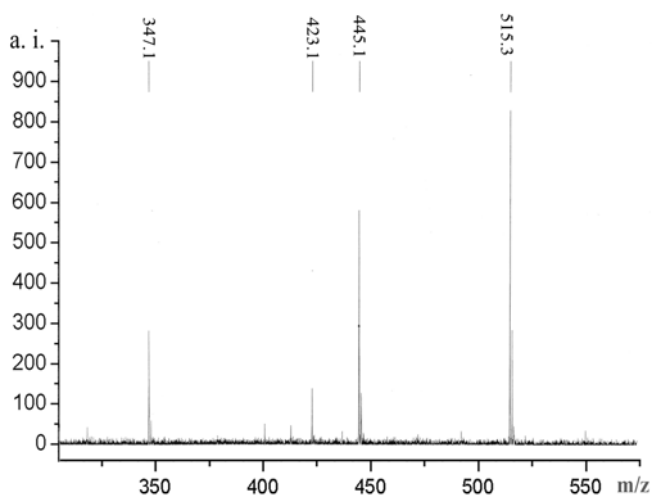


Figure S8 MALDI-TOF mass spectra of the thermal products. Experimental conditions: positive reflective mode, CCA + Na as matrix. The peaks at 347.1 and 515.3 corresponded to $(M_{\text{thiocoumarin dimmer}} + \text{Na})^+$ and $((R,R)\text{-}(-)\text{-trans-2,3-bis-(hydroxyldiphenylmethyl)-1,4-dioxaspiro[4.4]nonane} + \text{Na})^+$, respectively.

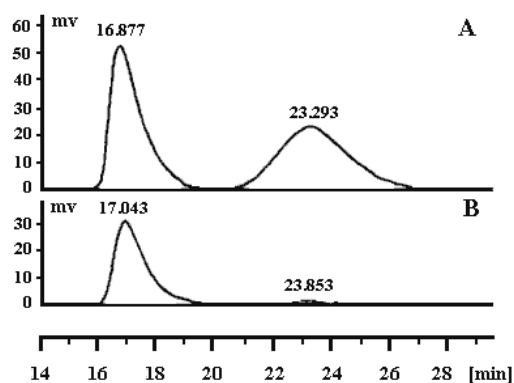
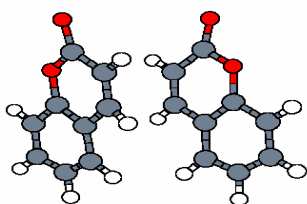


Figure S9. Chiral HPLC spectra (Chiralcel OJ column, hexane/2-propanol = 70:30, flow rate = 0.8 mL/min., $\lambda = 230$ nm) of racemic anti-head-to-head thiocoumarin dimmer (A) and the thiocoumarin dimmer obtained by thermal [2+2] reaction under vacuum ($>95\%$ ee) (B).

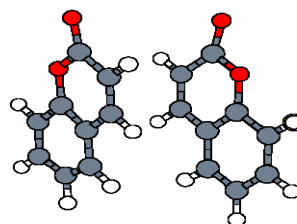
Theoretical Calculation Section:

In order to further identify the key role of (-)-TADDOL, both restricted and unrestricted density functional theory (DFT) were applied in the theoretical studies on the reaction mechanism of coumarin dimerization, in which restricted DFT was used for singlets and unrestricted DFT for higher multiplicities. B3LYP hybrid functional and a big basis set (6-31G**) were adopted in this work. Two models were built and studied in detail. As shown in Figure S11, model A was made of two coumarins and model B was constructed by two coumarins and two methanol molecules. The methanols in model B were added to mimic the hydrogen bonding between (-)-TADDOLs and coumarins. For each model, the calculations were carried out on four structures, namely, the reactant (structure 1), the bi-radical intermediate (structure a), the mono-bonded bi-radical intermediate (structure b or c), and the product (structure 2). The total energies and relative energies of all models were listed in Table S1, and a sketch of the reaction paths of coumarin dimerization was shown in Figure S12. From Table S1 and Figure S12, it could be clearly seen that, the pathway of model B was much favorable in energy over model A, because all structures of intermediates were relatively stable than those of model A. For example, comparing to the corresponding energy (47.0 kcal/mol) of structure a in model A, the relative energies (9.1 kcal/mol) of model B were much lower. It means, for model B, it is much easier to produce a bi-radical intermediate than model A. Such a step was very important to induce the reaction of coumarin dimerization. Moreover, structure c (the mono-bonded bi-radical intermediate) of model B was 16.2 kcal/mol lower than structure 1 (the reactant), which was also more stable than corresponding structure c for model A (12.3 kcal/mol lower than the reactant). Above results clearly indicated that the hydrogen bonds between coumarins and (-)-TADDOLs played a key role in stabilizing the reaction intermediates (namely, the bi-radical intermediate) of coumarin dimerization, and in turn, could help to start the reaction under a mild temperature.

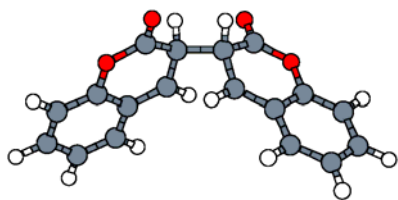
Model A: without H-bonding



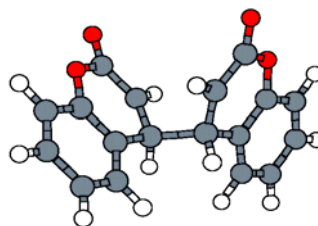
Structure 1: reactant



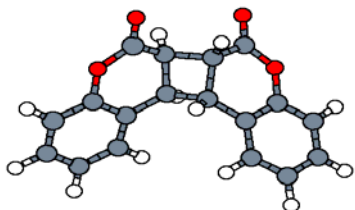
Structure a: bi-radical intermediate



Structure b: mono-bonded bi-radical
Intermediate

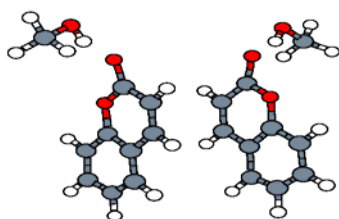


Structure c: mono-bonded bi-radical
intermediate

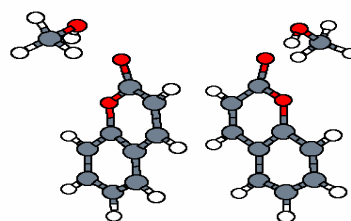


Structure 2: product

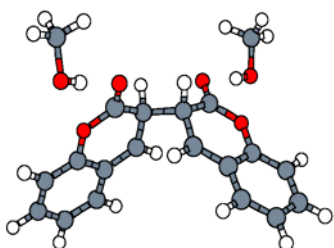
Model B: In the presence of H-bonding



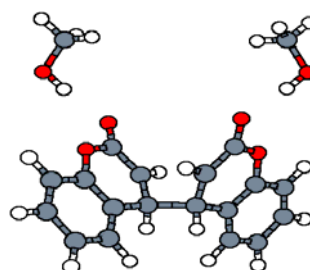
Structure 1: reactant



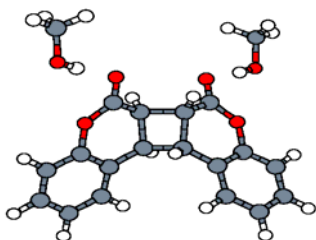
Structure a: bi-radical intermediate



*Structure b: mono-bonded bi-radical
intermediate*



*Structure c: mono-bonded bi-radical
intermediate*



Structure 2: product

Figure S10 Models used in theoretical calculations. All models were built from crystal structures ^[2], and optimized before carrying on single point energy calculations. For structures 1 and a, models were partially optimized, so that the original crystal structures were considered. And all the others were fully optimized.

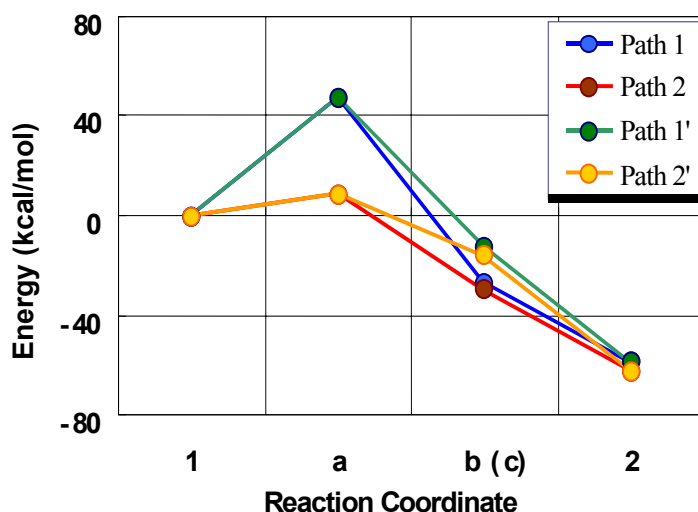


Figure S11 A sketch of the relative energies vs reaction paths (as described in Scheme 2) of coumarin dimerization without (model A) and with H bonds (model B). Path 1 (blue line) and path 2 (red line) represented the reaction paths via structure b of models A and B respectively, while path 1' (green line) and path 2' (yellow line) via structure c of models A and B, respectively. The detailed Structures of **1**, **a**, **b**, **c**, and **2** for models A and B were described in **Figure S11**.

Table S1. Energies along the reaction pathway of coumarin dimerization, with (model B) and without H bonds (model A)

Model A	Total energy	Relative energy*	Model B	Total energy	Relative energy*
	a.u.	kcal/mol		a.u.	kcal/mol
1	-993.9566754	0	1	-1225.4184529	0
a	-993.881832	47.0	a	-1225.40396	9.1
b	-993.9990342	-26.8	b	-1225.4658611	-29.7
c	-993.9762196	-12.3	c	-1225.4442848	-16.2
2	-994.0507054	-59.0	2	-1225.5177768	-62.3

* The relative energies were the energies of various structures as the energy of structure 1 was assigned to 0 kcal/mol.

References

- [1] (a) K. Tanaka, F. Toda, E. Mochizuki, N. Yasui, Y. Kai, I. Miyahara, K. Hirotsu, *Angew. Chem. Int. Ed.* 1999, 38, 3523-3525; (b) K. Tanaka, E. Mochizuki, N. Yasui, Y. Kai, I. Miyahara, K. Hirotsu, F. Toda; *Tetrahedron*, 2000, 56, 6853
- [2] All calculations in this work were carried out with Gaussian 98. Becke three-parameter hybrid functional with the non-local correlation provided by the Lee-Yang-Parr expression (B3LYP) was applied using 6-31G(3df, 3pd) basis set.
- A. D. Becke, *J. Chem. Phys.* 98, 5648(1993).
- C. Lee, W. Yang, and R. G. Parr, *Phys. Rev. B* 37, 785(1988).
- Gaussian 98, Revision A.11, M. J. Frisch, G. W. Trucks, H. B. Schlegel, G. E. Scuseria, M. A. Robb, J. R. Cheeseman, V. G. Zakrzewski, J. A. Montgomery, Jr., R. E. Stratmann, J. C. Burant, S. Dapprich, J. M. Millam, A. D. Daniels, K. N. Kudin, M. C. Strain, O. Farkas, J. Tomasi, V. Barone, M. Cossi, R. Cammi, B. Mennucci, C. Pomelli, C. Adamo, S. Clifford, J. Ochterski, G. A. Petersson, P. Y. Ayala, Q. Cui, K. Morokuma, P. Salvador, J. J. Dannenberg, D. K. Malick, A. D. Rabuck, K. Raghavachari, J. B. Foresman, J. Cioslowski, J. V. Ortiz, A. G. Baboul, B. B. Stefanov, G. Liu, A. Liashenko, P. Piskorz, I. Komaromi, R. Gomperts, R. L. Martin, D. J. Fox, T. Keith, M. A. Al-Laham, C. Y. Peng, A. Nanayakkara, M. Challacombe, P. M. W. Gill, B. Johnson, W. Chen, M. W. Wong, J. L. Andres, C. Gonzalez, M. Head-Gordon, E. S. Replogle, and J. A. Pople, Gaussian, Inc., Pittsburgh PA, 2001.
- [3] The models used in this work were adapted from the crystal structures of CSD.
- [4] Dr. J. Bian would like to acknowledge the grants funded by NSFC under project Nos. 20201002 and 20221101.